Interfacial mechanical behaviors of RC beams strengthened with FRP

Jiangdong Deng[1], Airong Liu[*2], Peiyan Huang[3] and Xiaohong Zheng[3]

[1]*College of Civil Engineering, Guangzhou University, Guangzhou 510006, China*
[2]*Guangzhou University-Tamkang University Joint Research Center for Engineering Structure Disaster Prevention and Control, Guangzhou University, Guangzhou 510006, China*
[3]*College of Civil Engineering and Transportation, South China University of Technology, Guangzhou 510640, China*

Abstract. FRP-concrete interfacial mechanical properties determine the strengthening effect of RC beams strengthened with FRP. In this paper, the model experiments were carried out with eight specimens to study the failure modes and the strengthening effect of RC beams strengthened with FRP. Then a theoretical model based on interfacial performances was proposed and interfacial mechanical behaviors were studied. Finite element analysis confirmed the theoretical results. The results showed that RC beams strengthened with FRP had three loading stages and that the FRP strengthening effects were mainly exerted in the Stage III after the yielding of steel bars, including the improvement of the bearing capacity, the decreased ultimate deformation due to the sudden failure of FRP and the improvement of stiffness in this stage. The mechanical formulae of the interfacial shear stress and FRP stress were established and the key influence factors included FRP length, interfacial bond-slip parameter, FRP thickness, etc. According to the theoretical analysis and experimental data, the calculation methods of interfacial shear stress at FRP end and FRP strain at midspan were proposed. When FRP bonding length was shorter, interfacial shear stress at FRP end was larger that led to concrete cover peeling failure. When FRP was longer, FRP reached the ultimate strain and the fracture failure of FRP occurred. The theoretical results were well consistent with the experimental data.

Keywords: interfacial mechanical behaviors; RC beams; FRP; model experiment; theoretical model; finite element analysis

1. Introduction

Fiber-reinforced polymer (FRP) has many advantages, such as high strength and high corrosion resistance. The strengthening of reinforced concrete (RC) beams by external bonding of FRP laminates is widely applied in civil engineering. Many researchers have studied the performance of RC beams strengthened with FRP.

Rostasy *et al.* (1992), Burgueno *et al.* (2001), Ahmed *et al.* (2001), Brena *et al.* (2003), Hag-Elsafi *et al.* (2004), Gao *et al.* (2006), Saxena *et al.* (2008), Said (2010), Attari *et al.* (2012), Mitolidis *et al.* (2012), Taleb and Salem (2015), Irshidat *et al.* (2016) found that the bearing

capacity of the strengthened RC beams had been greatly increased while the deflection decreased. FRP rupture after yielding of steel, FRP debonding and concrete-cover separation were common failure modes.

The behavior of the bond between FRP and concrete may be the most fundamental one to understand the behavior of the complete structural system and the strengthening mechanism because it plays a key role in the composite's performances and the reliability of RC structures after being strengthened (Protchenko *et al.* 2015). Many theoretical models of RC beams strengthened with FRP had been built.

Bizindavyi and Neale (1999) established the theoretical analysis model of the interface between FRP and concrete to study the distribution of interfacial bond stress, calculate anchorage length of FRP, and analyze the influences of concrete strength and the thickness of bonding layer on the interfacial strength. Based on the tensile shear thermostimulated tests performed on the interface, Ferrier and Hamelin (2002) proposed a methodology to evaluate the allowable shear stress of the interface. Guenaneche *et al.* (2010) studied interfacial stresses in RC beams strengthened with bonded composite laminates according to linear elastic theory and explicitly explored the interface slip effect on the structural performance based on the consideration of both the adherend shear deformations and the time-dependent deformations. Bennati *et al.* (2012) proposed a mechanical model, whereby the beam and FRP strip were modeled according to classical beam theory, while the adhesive and its neighboring layers were modeled as an interface with a piecewise linear constitutive law defined within three intervals. Bocciarelli and Pisani (2015) proposed a numerical method, in which the FRP sheets were separated from the reinforced concrete substructure by displaying the interface stresses which were taken into account by means of the corresponding interface slips (which are the primary unknowns). Compatibility equations were then imposed at the interface in order to restore the behavior of the externally reinforced beam.

As for theoretical models of different failure modes, Teng and Yao (2007) proposed a simple and rational prediction model of debonding failure at the plate end based on available test results. Rasheed and Motto (2010) developed the exact and approximate sets of closed form equations to design the reinforced strengthened rectangular sections which failed in the forms of FRP rupture or cover delamination. Zhang and Teng (2014) presented a novel FE approach to predict end cover separation failures in strengthened RC beams. Al-Zaid Rajeh *et al.* (2012), Bilotta *et al.* (2013) proposed rational models to analyze the maximum axial strain in FRP at the onset of intermediate debonding failure.

The existing research reveals the complexity of the mechanical behaviors of FRP-strengthened RC beams, and the interfacial mechanical behaviors are the control factors of the strengthened RC beams. At present, the interfacial failure mechanism and generally accepted mechanical model are not available. The plane section assumption is widely adopted to analyze RC beams strengthened with FRP in engineering practices, but this assumption neglects interfacial mechanical behaviors and may lead to some errors. Therefore, it is necessary to further study the interfacial mechanical behaviors of RC beams strengthened with FRP.

In this paper, on the basis of model experiments, the failure modes and the load-deflection curves of RC beams strengthened with FRP were analyzed. Moreover, a new theoretic model of RC beam strengthened with FRP determined by the FRP-concrete interfacial performances was proposed and the interfacial mechanical behaviors, such as the stress distribution, FRP stress and the key influence parameters were explored. The model was confirmed by finite element analysis. Then the calculation formulas of stresses at FRP end and mid span were proposed, and the causes of the concrete cover peeling failure at FRP end and FRP fracture at the mid span in experiments

Table 1 The uniaxial compressive strength of concrete

No.	Axial compressive strength f_C (MPa)	Elastic modulus Ec (GPa)	Poisson's ratio, v
1	37.92	25.03	0.19
2	39.55	25.31	0.19
3	37.76	25.16	0.21
Averages	38.41	25.18	0.20

Table 2 Mechanical properties of steel bars

Grade	Diameter	Applications	Yield strength, f_y (MPa)	Ultimate strength, f_u (MPa)	Elongation percentage, δ (%)	Elastic modulus, E_S (GPa)
Grade-I	8	Hanger bars and stirrups	310	500	23	194
Grade-II	10	Main reinforcement	328	444	24	200

were well studied. The mechanical behaviors of FRP, interface and RC beam can be easily determined with this model. The related results may be used in theoretical analysis and engineering practices of RC beams strengthened with FRP.

2. Experimental investigation

2.1 Concrete materials

In the test, the concrete was prepared with Portland cement, water, locally available sand, and crushed granite rock according to the weight ratio of 1.0:0.5:2.06:3.66. The concrete prism specimens (150×150×300 mm) were used to test the compressive strength. Testing equipment is a 2000-KN press machine. The testing results are provided in Table 1.

2.2 Steel materials

In the test, steel bars can be divided into three types: the main reinforcement, hanger steel, and stirrup. The main reinforcement is Grade-II steel bar with the diameter of 10 mm. The hanger bars and stirrups are Grade-I steel bar with the diameter of 8 mm. Mechanical properties of the steel bars are shown in Table 2.

2.3 FRP and bonding materials

The adopted carbon fiber is T300-3K, with the tensile strength of 3500 MPa and the elastic modulus of 400 GPa. The substrate material of FRP is epoxy resin. A single layer of FRP sheet of 0.23 mm thickness was used to strengthen RC beams. The main mechanical properties of FRP are provided in Table 3 and the strain-stress curves are shown in Fig. 1. The FRP rupture strength is much higher than that of the steel bar, while its ductility is lower than the later. The elastic modulus of FRP is close to that of steel bar. When the steel bat reaches the yield point, FRP is in its lower stress state. So FRP strength is fully used after the steel bars yield.
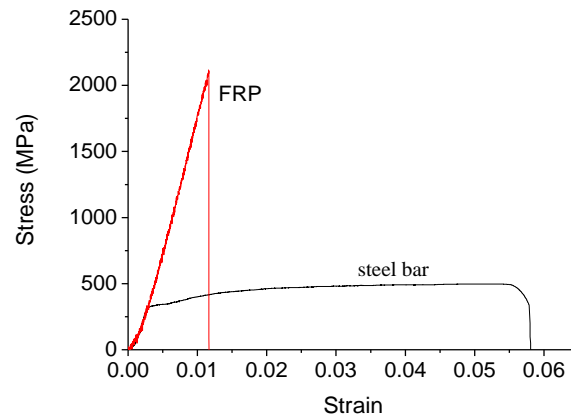
Fig. 1 The strain-stress curves

Table 3 The mechanical properties of FRP

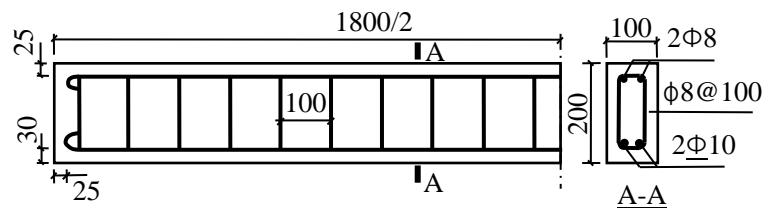| Thickness (mm)	Width (mm)	Tensile strength (MPa)	Elastic modulus (GPa)	density (g/cm^3)
0.23	100	2100	240	1.76

Fig. 2 Steel bars of concrete beam (unit: mm)

The epoxy resin was used to stick FRP on RC beam bottom surface. The application temperature of epoxy resin is ranged between -30 ℃ and +100 ℃. The shear strength of epoxy resin is 14 MPa.

2.4 RC beam strengthened with FRP

The size of RC beam is 1800×100×200 mm (Length×Width×Height). Two main reinforcements with diameter of 10mm were placed on the tensile side; two hanger bars with diameter of 8mm were placed on the compressive side of the beam; and the diameter and spacing of stirrups is 8mm and 100 mm, as shown in Fig. 2.

The FRP sheet is 0.23 mm thick and 100 mm wide, which is the same width as the RC beam.

The bonding steps of FRP are described as follows:

1) The adhesive surface of RC beam was polished to make the surface smooth;

2) Surface dust was removed with compressed air; the cotton yarn and acetone were used to clean the adhesive surface;

3) Adhesive resin was evenly daubed on the RC beam bottom surface and the coating thickness was between 0.1 mm and 0.2 mm;

4) FRP was bonded on the bottom surface of RC beam;

Fig. 3 FRP strengthened RC beam

Table 4 Details of each specimen

Beam No.	A1	A2	B1	B2	B3	C1	C2	C3
FRP length (m)	0	0	0.8	0.8	0.8	1.6	1.6	1.6
Reinforcement ratio	0.92%	0.92%	0.92%	0.92%	0.92%	0.92%	0.92%	0.92%
FRP ratio	0	0	0.14%	0.14%	0.14%	0.14%	0.14%	0.14%
Main steel bars tensile force (N)	51496	51496	51496	51496	51496	51496	51496	51496
FRP tensile force (N)	0	0	48300	48300	48300	48300	48300	48300
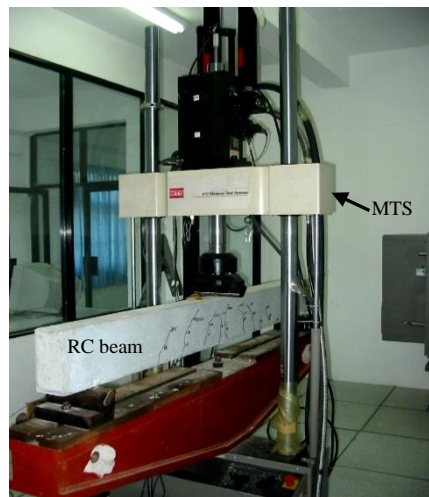
Fig. 4 Testing system for three-point bending specimen

5) FRP was compressed by the compression tool for 48 hours at room temperature.

FRP strengthened RC beam is shown in Fig. 3 and the black part is FRP.

This experiment focused on the effect of FRP length on the mechanical performances of the beams. Eight specimens were divided into 3 groups. We mainly analyzed the effects of different FRP lengths on the mechanical behaviors of the strengthened RC beams. Group A had two RC beam specimens which were not strengthened with FRP. Group B included 3 specimens and the FRP bonding length was half of the beam span. Group C had 3 specimens and the length of FRP covered the full span of the beam. The details of each specimen are summarized in Table 4.

According to Code for design of Concrete Structures (GB-50010), the reinforcement ratio of RC beam is 0.92%, which exceeds the minimum reinforcement ratio, 0.2%. The depth of compression zone of the strengthened RC beam is 32.3 mm, which is less than the balanced depth of compression zone of $\xi_b h_0$=91.7 mm to avoid over-reinforced failure. The total tensile force of

main steel bars is 51.5 kN and the FRP ultimate tensile force is 48.3 kN.

2.5 Loading devices

The adopted testing device is the MTS testing machine, as shown in Fig. 4. The load was applied according to the three-point bending method and the distance between the two supports was 1.6 m. In this test, the displacement-controlled mode at the speed of 0.01 mm/s was used to control the loading process until the specimen was destroyed. The load and the displacement data were recorded by MTS.

One strain gage was attached to the bottom surface of FRP at midspan. The strain data were continuously acquired with a strain indicator and the sampling frequency was 10 Hz.

3. Results

3.1 Failure mode

The RC beam specimens of Group A were not strengthened with FRP and the failure mode had the typical failure characteristics of a reinforced concrete beam. The concrete cracks initiated at the midspan of RC beam along the applied loading, then propagated slowly before the reinforced steel bar was yielded. After the steel bar was yielded, the cracks developed rapidly. Finally, the steel bar was broken thoroughly and a small quantity of concrete was crushed at the loading position of the top surface of RC beam, as shown in Fig. 5.

The failure mode of the specimens of Group B is shown in Fig. 6. As can be seen, along with the loading, the incline concrete crack appeared at the FRP end because of the interfacial shear stress. When the concrete shear crack reached the reinforced steel bars, it propagated along the reinforcement. At last from the incline crack at FRP end the concrete cover was pulled down and the whole specimen was destroyed. Concrete cover peeling caused by the interfacial shear stress was the typical character of this failure mode.

The failure mode of the specimens of Group C is shown in Fig. 7. Before the failure, local concrete spalling occurred at the interface. Finally, FRP was pulled off at a weak position near the midspan, and the strengthened RC beam was destroyed suddenly. The failure mode could be

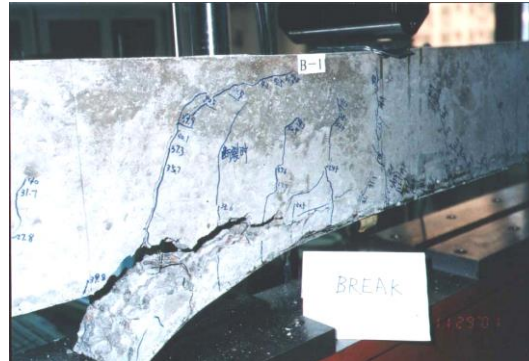Fig. 5 Failure mode of the specimens of Group A

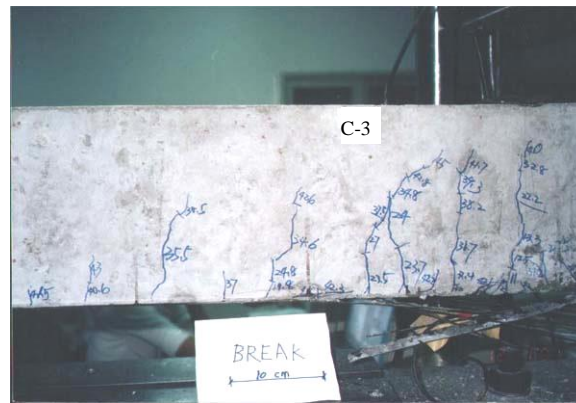Fig. 6 Failure mode of the specimens of Group B

Fig. 7 Failure mode of the specimens of Group C
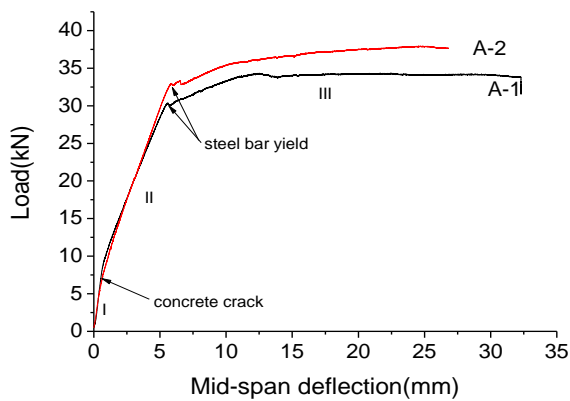

Fig. 8 Load displacement curves of the specimens of Group A
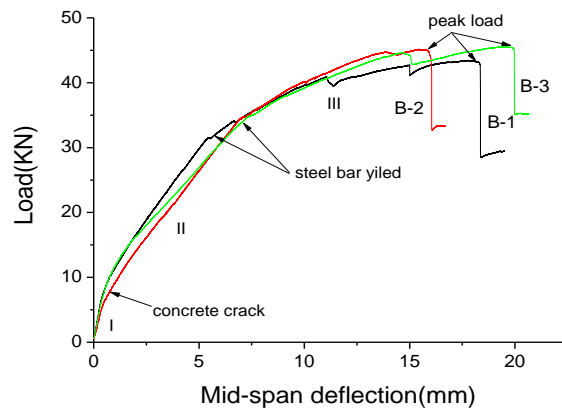

Fig. 9 Load displacement curves of the specimens of Group B

classified as the brittle failure. After the specimens failed, it was observed that the main crack width was less than 1 mm and other cracks were fine and dense.
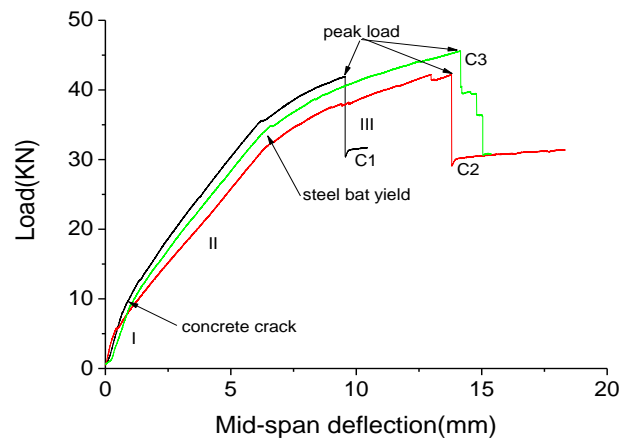
Fig. 10 Load displacement curves of the specimens of Group C

3.2 Force-displacement curve

The load-displacement curves of Group A to C are shown in Figs. 8-10, respectively. The load-displacement curves can be divided to 3 stages. Stage I ends when concrete cracks; Stage II ends when steel bar yields; Stage III ends just before the failure of the strengthened RC beam.

Group A shows the load-displacement curves of typical reinforced concrete beams. An obvious turning point is observed on the curves when the yielding of the reinforced steel bar occurs. And after the yield load, the plastic deflection is about four times the yield deflection. So the plastic deformation capability of RC beam is high, but the beams strengthened with FRP destroyed just after the peak load.

The average yield load of RC beams strengthened with FRP in Group B is 33.8 kN. The average yield load of Group A is 31.9 kN, which is close to that of Group B. The average yield displacement of Group B is 6.67 mm, which is also consistent with that of Group A. For the ultimate bearing capacity, Group B specimens are tested to be 44.0 kN, which is improved by 23.2% compared with ultimate load of Group A. The midspan deflection of Group B in the final failure reaches 18.1 mm, which is 61.0% of non-strengthened beams in Group A.

The average yield load and yield displacement of Group C is 34.4 kN and 6.58 mm. The ultimate bearing capacity of Group C is 43.2 kN, which is close to that of Group B. For those Group C beams, the ultimate deflection at midspan is 12.5 mm, which is 30.9% lower than that of Group B and 57.7% lower than that of Group A.

For better understanding of the effect of bonded length of FRP, the variation of the ultimate load with FRP bonding length is plotted in Fig. 11. After strengthened by FRP, the bearing capability of RC beams has been greatly improved, but the effect of FRP length on the yield load is insignificant. The improvement in the bearing capacity of RC beam mainly appears in Stage III as shown in Table 5.

The variation of the deflection with FRP bonding length is shown in Fig. 12. With the increase of FRP length, the ultimate deformation is decreased, indicating that the ductility of the strengthened members is reduced. The yield deflection of different FRP length is almost the same.

Because RC beams in service are often subjected to heavy load before strengthening, the strengthening effect is suspected that FRP may not reach the ultimate strength for a long time.
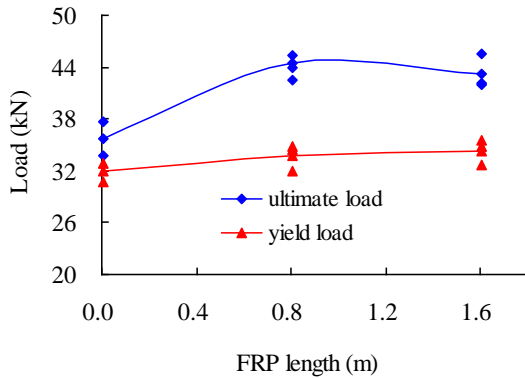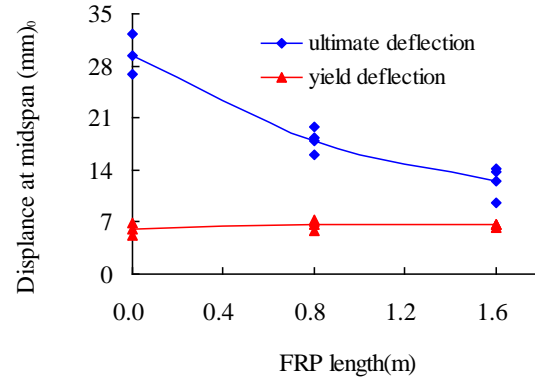
Fig. 11 Variation of load with FRP length

Fig. 12 Variation of deflection with FRP length

Table 5 Flexural stiffness of different stage (kN·m)

Beam No.	Stiffness of Stage I	Deflection of stage II (mm)	Load of stage II (kN)	Stiffness of stage II	Stiffness of stage III	Ultimate deflection (mm)	Ultimate load (kN)	Ultimate stiffness
A1	863.4	5.26	30.8	429.6	9.5	32.25	33.8	89.4
A2	843.4	6.78	32.9	351.7	20.0	26.80	37.6	119.7
B1	942.7	5.77	32.0	368.3	71.5	18.34	42.5	197.7
B2	889.9	7.22	34.8	359.9	89.5	15.99	44.0	234.8
B3	967.1	7.02	34.5	322.8	72.4	19.89	45.4	194.8
C1	870.1	6.30	35.6	407.3	165.4	9.55	41.9	374.4
C2	866.7	6.72	32.6	366.3	115.7	13.80	42.2	260.9
C3	747.6	6.72	34.9	384.2	122.7	14.16	45.6	274.8

According to experimental data, even when the beam reaches the yield point, because of high plastic deformation capability of RC beam, after being strengthened, the FRP strength can be fully used.

3.3 Flexural stiffness

Flexural stiffness in different stages is the secant stiffness between the starting point and endpoint, as shown in Table 5.

It can be seen that the flexural stiffness of Stage I of different beams is similar to that of Stage II. The stiffness in Stage III and the ultimate stiffness of non-strengthened beams are smaller than that of the strengthened beams. The longer of FRP results in the higher flexural stiffness.

4. Theory and FEM analysis

4.1 FRP-concrete interface stress calculation

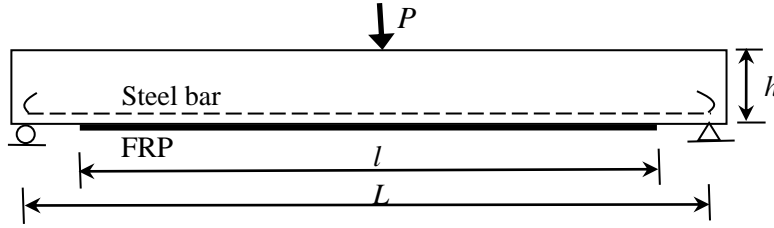The three-point bending specimen is shown in Fig. 13. RC beam strengthened with FRP can be

Fig. 13 Three-point bending specimen of RC beam strengthened with FRP
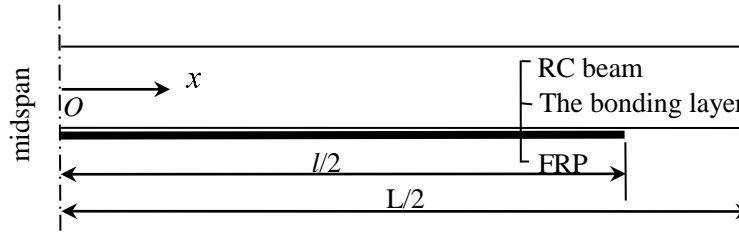

Fig. 14 Analysis model of RC beams strengthened with FRP

divided into 3 parts: RC beam, bonding layer, and FRP. Due to the symmetry, only half of the component is analyzed. The established coordinates are shown in Fig. 14.

In order to simplify the calculation, the following assumptions are adopted:

1) The interfacial adhesion is good and the stress is zero in the initial state;

2) Because the FRP is thinner, FRP can only bear the force along the fiber direction, and FRP cannot bear the load in the direction perpendicular to the FRP plane due to the absence of carbon fiber.

3) In the cross section of FRP, the stress distribution is uniform.

Since the plane section assumption of RC beam strengthened with FRP has not been generally recognized, in this paper, this assumption is not adopted in the calculation of the force of each member and the RC beam is analyzed as a whole elastic body.

Due to that the difference between thickness of carbon fiber sheet and height of RC beam reaches several orders of magnitude, the effect of carbon fiber sheet on the neutral axis of the strengthened RC beam is negligible and this effect is not considered in present analysis. Therefore, the deformation of beam bottom surface meets the following equation

$$\frac{du_c}{dx} = \frac{Ph}{4B_s}(\frac{L}{2} - x) - \frac{F(x)h^2}{4B_s}, \tag{1}$$

where P is the load applied on the RC beam; $F(x)$ is FRP tensile force at x position; L is the span length; h is the height of RC beam; B_s is the flexural rigidity of RC beam; u_c is the displacement of bottom surface of RC beam and it is a function of x.

According to the displacement coordination condition, the displacements of concrete bottom surface and FRP are the displacements of top and bottom surfaces of adhesive layer, respectively. For the adhesive layer, the shear force is
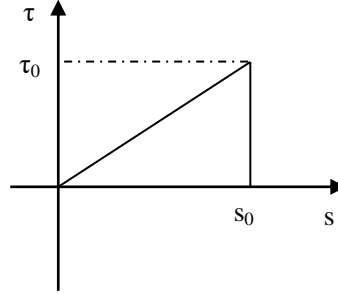
$$\tau(x) = H(u_c - u_f), \tag{2}$$

Fig. 15 Bond-slip model of the interface between FRP and concret

where u_f is FRP displacement; H is the interfacial bond-slip constitutive parameter.

According to the literature, many FRP-concrete interface bond-slip models (Neubauer and Rostasy 1999, Chen and Teng 2001, Lu *et al.* 2005, Diab and Wu 2007, Zhou *et al.* 2010, Lin and Zhang 2013, Ko *et al.* 2014) have been established, but most of them are quite complex. The linear bond-slip model (Fig. 15) is relatively simple, precise and widely recognized (Lu and Zheng 2004). The mechanical expression of the linear bond-slip model is expressed as

$$
\begin{aligned}
\tau &= \tau_{\max}\left(\frac{s}{s_0}\right) & s \leq s_0 \\
\tau &= 0 & s > s_0
\end{aligned}
$$
(3)

Through the experiment of 70 specimens, Neubauer and Rostasy (1999) gave the bond-slip parameter: $H = 8.91 \times 10^3 f_t$, where f_t is the concrete tensile strength.

As for FRP, the relationship between the force and the deformation can be expressed as

$$
F(x) = E_f t_f b\left(\frac{du_f}{dx}\right),
$$
(4)

where E_f is the elastic modulus of FRP; t_f is the thickness of FRP; b is the width of FRP or the width of the RC beam.

For FRP, according to the force balance of the micro segment, we get

$$
\frac{dF(x)}{dx} = -\tau(x)b .
$$
(5)

According to Eqs. (1), (2), (4), and (5), Eq. (6) is obtained as

$$
\frac{d^2 F(x)}{dx^2} - C_1^2 F(x) + C_2\left(\frac{L}{2} - x\right) = 0,
$$
(6)

where $C_1^2 = \dfrac{B_t H}{B_s E_f t_f}$; $C_2 = \dfrac{PHhb}{4B_s}$. The stiffness of the strengthened member is $B_t = B_s + 0.25 E_f t_f h^2 b$, in which the second term is the increase of RC beam stiffness caused by FRP.

Boundary conditions:

At the end of FRP: $F(\dfrac{l}{2}) = 0$;

At midspan: $\dfrac{dF(0)}{dx} = 0$;

Then the solution of Eq. (6) can be simplified as

$$F(x) = \frac{C_2}{C_1^2}\left(\frac{L}{2} - x\right) + \frac{C_2}{C_1^3\left(1 + e^{C_1 l}\right)}\left(e^{C_1 x} - e^{C_1(l-x)}\right) - \frac{C_2}{2C_1^2\left(1 + e^{C_1 l}\right)}(L - l)\left(e^{C_1\left(\frac{l}{2} + x\right)} + e^{C_1\left(\frac{l}{2} - x\right)}\right), \quad (7)$$

where l is the length of FRP.

According to Eqs. (5) and (7), the interface shear stress can be obtained as

$$\tau(x) = \frac{C_2}{bC_1^2} - \frac{C_2}{bC_1^2\left(1 + e^{C_1 l}\right)}\left(e^{C_1 x} + e^{C_1(l-x)}\right) + \frac{C_2}{2bC_1\left(1 + e^{C_1 l}\right)}(L - l)\left(e^{C_1\left(\frac{l}{2} + x\right)} - e^{C_1\left(\frac{l}{2} - x\right)}\right). \quad (8)$$

In the following analysis, the values of each variable in Eq. (8) are provided in Table 6.

4.2 Finite element simulation

Due to the symmetry, half of the member was selected to establish three-dimensional FEA model, as shown in Fig. 16. The model was built in accordance with the specimens used in the model test. The size of FE model of such half RC beam was 0.8 m×0.1 m×0.2 m (length×width×

Table 6 Values of the parameters

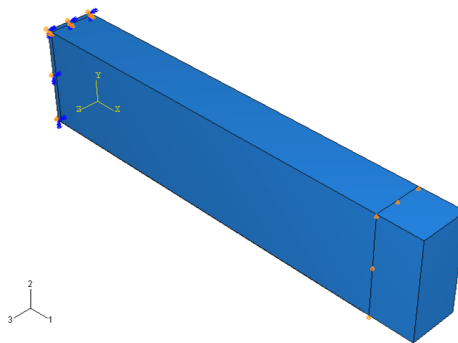| The member length, L	The length of FRP, l	The tensile strength of concrete, ft	Bond slip parameter, H	Concrete elastic modulus
1.6 m	1.2 m	3.4 MPa	3.03×10^{10} N/m	25 GPa
FRP elastic modulus, Ef	FRP thickness, tf	mid-span deflection, f	The thickness of concrete beam, h	The width of concrete beam, b
240 GPa	2.3×10^{-4} m	10 mm	0.2 m	0.1 m

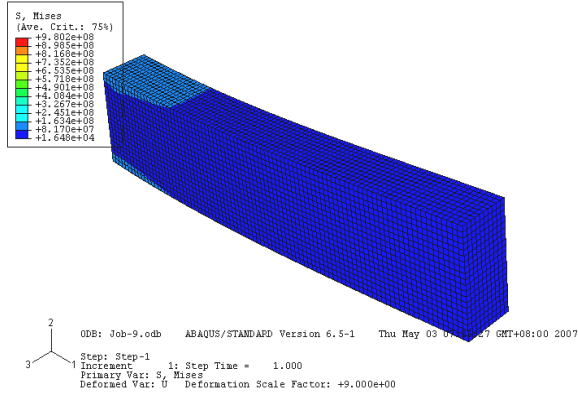Fig. 16 Three-dimensional FEM model for RC beam strengthened with FRP

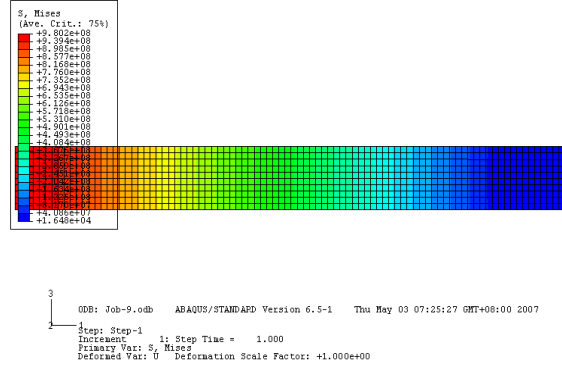Fig. 17 Distortion of the RC beam strengthened with FRP

Fig. 18 Stress contour in FRP

height). The lengths of FRP bonded on RC beam included 0.8 m, 0.6 m, and 0.4 m, which were respectively equivalent to the full span, 3/4 span, and 1/2 span. The thickness of FRP is 2.3×10^{-4} m, and the width of FRP is 0.1 m. The thickness of adhesive resin layer between the RC beam and FRP is 1.5×10^{-4} m.

In order to jointly bear force and deformation, the three parts-the RC beam, FRP and the adhesive layer were set as a whole part. The nodes and elements of the three parts were completely contacted in the analysis. Because the elements were also contacted, compared with the coupling displacement method at the node, this method can simulate the actual situation in a better way. The symmetrical constraint was applied on the left section of the model, and the vertical displacement constraint was applied on the section which was 0.8 m away from the left, as shown in Fig. 16.

The elastic modulus and Poisson's ratio of concrete are 25 GPa and 0.19, respectively. The elastic modulus of epoxy resin is calculated by $E_r = 2(1+v) \times H \times t_r$ (Cheng and Zhu 2005) and Poisson's ratio is 0.42. v and t_r are the Poisson's ratio and the thickness of the epoxy resin. The elastic modulus and Poisson's ratio of FRP are 240 GPa and 0.22, respectively.

The software ABAQUS was used for finite element analysis. Three-Dimensional Linear Full-Integration Element C3D8 was used for the simulation of concrete and FRP. The adhesive layer was simulated with the linear full-integration bonding element COH3D8. In order to improve the calculation precision, a fine analysis was conducted and the element size was set to be 5 mm.

The displacement mode was adopted in the loading process. The displacement is divided into 10 steps and each step is 0.001 m. Finally the mid-span deflection of 10 mm is applied on the strengthened beam, which is consistent with the external load in the theoretical model.

The deformation of the model and the stress distribution on FRP are shown in Fig. 17 and Fig. 18.

4.3 Interfacial behaviors of theoretical analysis and finite element simulation

Under different lengths of FRP, the theoretical results of interfacial shear stress (Eq. (8)) are compared with those from finite element analysis, as shown in Fig. 19 to Fig. 21.

The interfacial shear stress near the midspan and FRP end is changed dramatically, whereas in other positions it is changed smoothly. The interfacial shear stress at FRP end is very large when
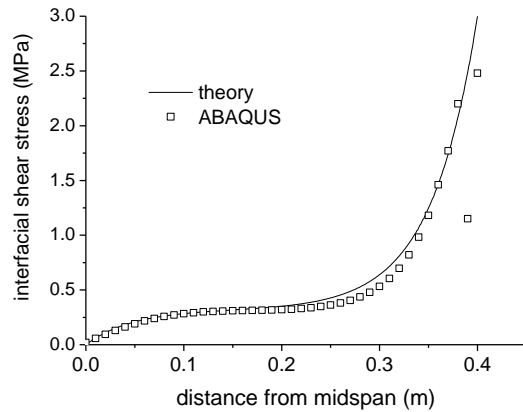
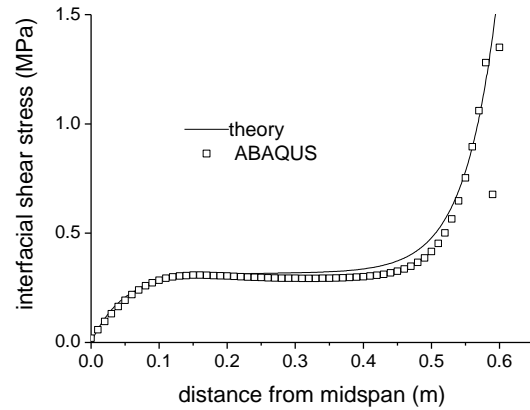Fig. 19 Interfacial shear stress under FRP length of 0.8 m

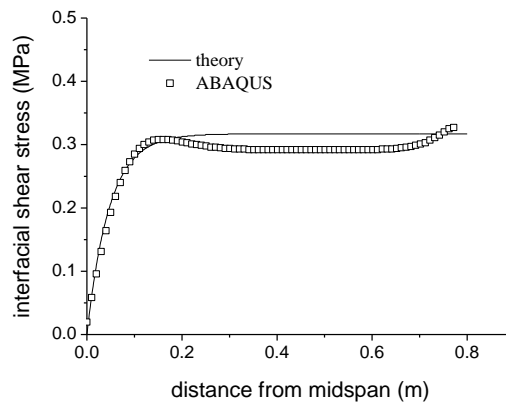Fig. 20 Interfacial shear stress under FRP length of 1.2 m

Fig. 21 Interfacial shear stress under FRP length of 1.6 m

the FRP length is 0.4 m or 0.6 m. The shorter the bonded FRP length means the larger the interfacial stress at FRP end. When the bonding length of FRP is equal to the span, the interfacial shear stress at FRP end is not greatly increased.

The bond slip parameter *H* and FRP thickness are key influencing factors of the interfacial mechanical properties. When FRP length is 0.8 m, the interfacial shear stress under different parameters is shown in Figs. 22 and 23. The higher bond slip parameter results in the larger changing rate of interfacial shear stress at midspan and FRP end. With the increase in FRP thickness, the interfacial shear stress increases.

Based on Eq. (7), theoretical FRP stress along the length is contrasted with the results simulated by ABAQUS, as shown in Fig. 24. With the decrease in FRP length, FRP stress at FRP end increases more rapidly. When FRP length is 0.8 m, the stress transfer distance is 0.2 m from FRP end. FRP stress under different FRP length of 0.8 m-1.6 m is similar at midspan.

At FRP end, because of the material discontinuity, local discontinuous jumping appears in the finite element simulation results. On the whole, the interfacial stress and FRP stress obtained through theoretical calculation are basically consistent with that obtained through ABAQUS simulation, so the theoretical model has higher precision.
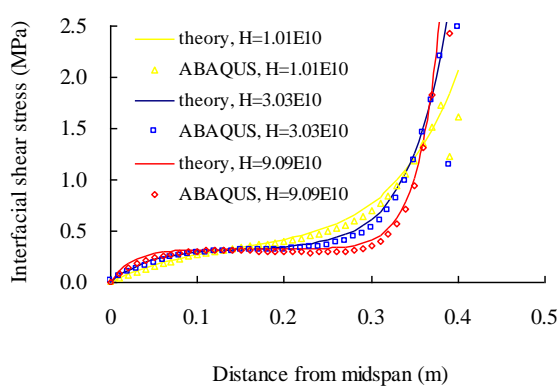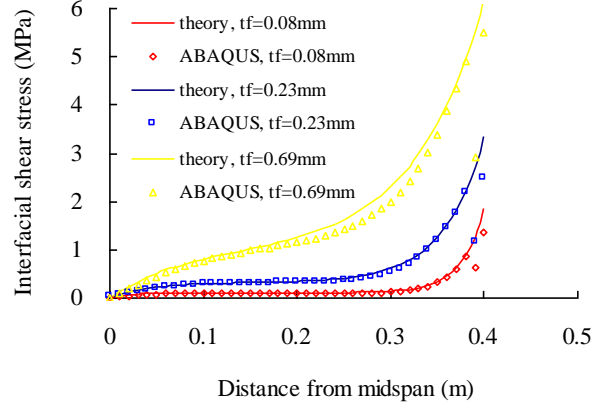
Fig. 22 Effect of bond slip parameter H on interfacial shear stress

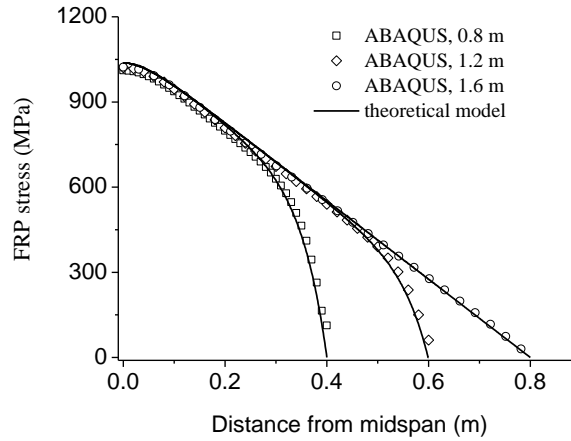Fig. 23 Effect of FRP thickness on interfacial shear stress

Fig. 24 FRP stress under different FRP lengths

5. Theoretical analysis on the failure in the experiment

5.1 Interfacial shear stress at FRP end

For the specimens of Group B, peeling failure of the concrete cover occurred. According to Eqs. (5) and (7), the interface shear stress at FRP end is

$$\tau(\frac{l}{2}) = \frac{C_2}{bC_1^2} - \frac{2C_2}{bC_1^2\left(1+e^{C_1 l}\right)}e^{C_1\frac{l}{2}} + \frac{C_2}{2bC_1\left(1+e^{C_1 l}\right)}(L-l)\left(e^{C_1 l}-1\right). \tag{9}$$

The midspan deflection is 18 mm, which is the same as the average deflection of Group B. FRP length is 0.8 m. Then the variations of the interfacial shear stress at FRP end with key factors including FRP length, FRP tensile stiffness, thickness of epoxy resin, flexural stiffness of the strengthened beam are shown in Fig. 25 to Fig. 28, respectively.
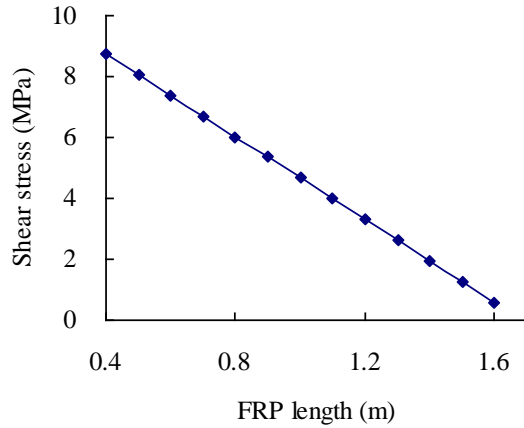
Fig. 25 The effect of FRP length on the interfacial shear stress at FRP end
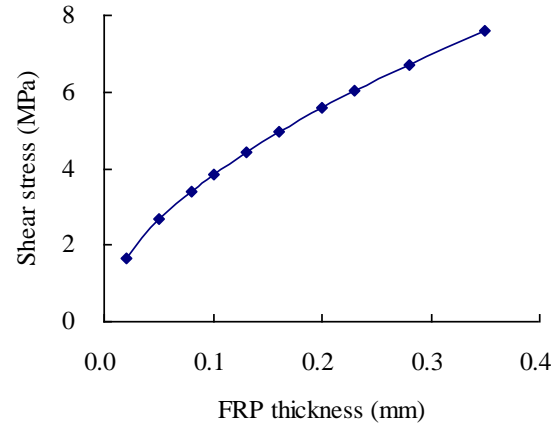

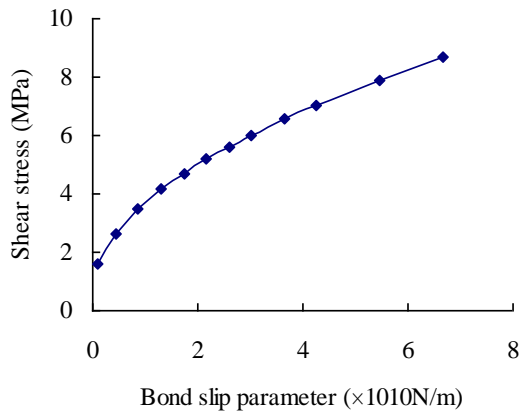Fig. 26 The effect of FRP thickness on the interfacial shear stress at FRP end

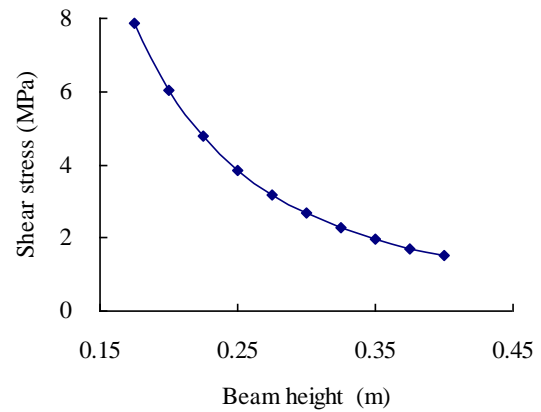Fig. 27 The effect of bond slip parameter on the interfacial shear stress at FRP end

Fig. 28 The effect of beam height on the interfacial shear stress at FRP end

As can be seen in Fig. 25, when the FRP length l is shorter than the beam length L, the interfacial shear stress at FRP end is large, and the shear stress at FRP end increases rapidly with the decrease of FRP length. When FRP length is 0.8 m, the interfacial shear stress at FRP end reaches 6.0 MPa, which reachs the shear strength of concrete (0.15 f_c=5.8 MPa). This can explain the failure mode (peeling of concrete cover) of the Group B in the experiment. With the increase of FRP thickness and bond slip parameter, the interfacial shear stress at FRP end increases (Figs. 26, 27). However, with the increase of RC beam height, the interfacial shear stress at FRP end decreases (Fig. 28).

5.2 FRP force at midspan

The failure mode of Group C is the FRP fracture at midspan, so FRP strain at midspan is analyzed below.

According to Eq. (7), if the length of FRP is longer, FRP force at midspan is
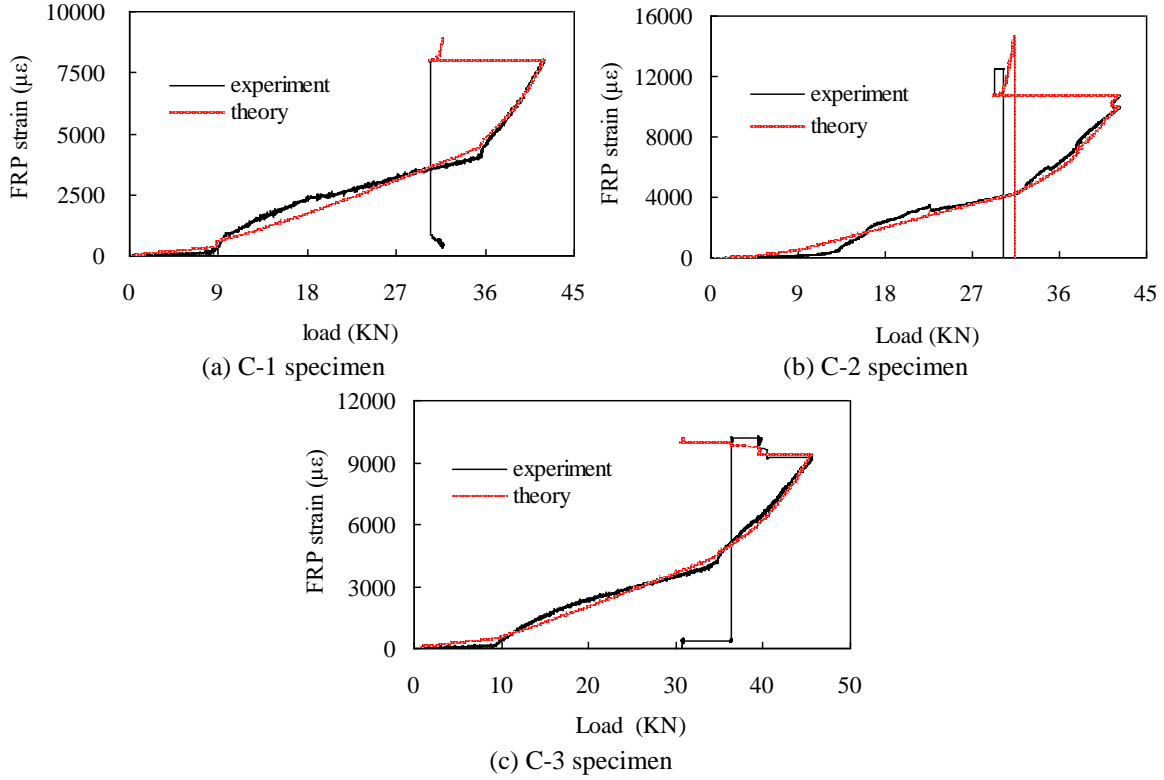
(a) C-1 specimen

(b) C-2 specimen

(c) C-3 specimen

Fig. 29 Relationship curves between FRP strain and load

$$F(0) = \frac{C_2 L}{2C_1^2} - \frac{C_2}{C_1^3} . \tag{10}$$

Omitting the small quantity, Eq. (10) can be simplified as

$$F(0) = \frac{P E_f t_f h b L}{8B_t} . \tag{11}$$

FRP strain ε_f at midspan is

$$\varepsilon_f = \varepsilon(0) = \frac{PhL}{8B_t} . \tag{12}$$

The above FRP strain analysis is based on the elasticity theory. However, in real engineering and experiment, there are cracks in RC beam. The phenomenon of stress concentration and neutral axis rising inevitably exist in the crack area, leading to the increase of FRP stress. In the actual situation, considering the influence of cracks in concrete, Eq. (12) is modified as

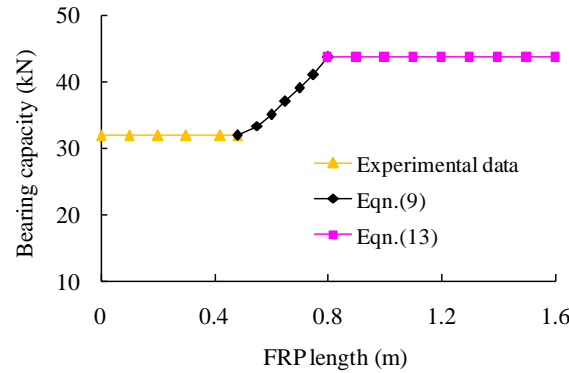$$\varepsilon_f = \phi \frac{PhL}{8B_t} \tag{13}$$

Fig. 30 Relationship between bearing capacity and FRP length

where ϕ is the influence coefficient of concrete cracks at midspan.

At Stage I, concrete cracks did not occur, so $\phi=1.1$; at Stage II, $\phi=1.55$. At Stage III, ϕ is 2.2, 1.9, and 1.4 for each beam of Group C. As shown in Fig. 26, the calculation curves are consistent with experimental curves of each specimen.

Based on the theoretical calculation, the average FRP strain of Group C beams is 9398 $\mu\varepsilon$, which reaches FRP fracture strain. This can explain FRP fracture of Group C in the experiment.

5.3 Bearing capacity of RC beam strengthened with FRP

According to experimental data and theory model, the bearing capacity of RC beam strengthened with FRP is determined by FRP length, as shown in Fig. 30.

It can be seen that when the FRP length is less than 0.48 m, after the concrete cover peeling at FRP end occurs, the RC beam can bear more loads until the yield point. When FRP length is between 0.48 m and 0.8 m, the concrete cover peeling occurs after the yield point of RC beam and the bearing capacity of the strengthened beam can be calculated by Eq. (9). When FRP length is more than 0.81 m, the bearing capacity can be calculated by Eq. (13) because FRP ruptures at midspan.

6. Conclusions

In this paper, the interfacial mechanical behaviors of RC beams strengthened with FRP were studied. The conclusions are summarized as follows:

1) RC beams strengthened with FRP have three loading stages. At Stage I and Stage II, the load, deflection and stiffness are similar, and FRP strengthening effect is mainly exerted at Stage III after the yield of steel bars. The ultimate bearing capacity and the ultimate stiffness of RC beam strengthened with FRP are much higher than that of the non-strengthened RC beams. When the length of FRP is more than 1/2 of the span, the effect of FRP bonding length on the ultimate bearing capacity is not significant. However, the ultimate displacement of FRP-strengthened RC beams is lower than that of the non-strengthened RC beams due to the sudden failure of FRP, and the longer FRP results in the smaller ultimate displacement.

2) A new theoretic model of RC beam strengthened with FRP determined by the FRP-concrete

interfacial performances was proposed. The mechanical formulae of the interfacial shear stress and FRP stress were established and the key influence factors were studied. The theoretical model was confirmed by FEA.

3) According to the theoretical analysis and experimental data, the calculation methods of interfacial shear stress at FRP end and FRP strain at midspan were proposed.

4) When FRP bonding length was shorter, interfacial shear stress at FRP end was larger, thus leading to concrete cover peeling failure. When FRP was longer, FRP reached the ultimate strain and the fracture failure of FRP occurred. The theoretical results were well consistent with the experimental phenomena. Based on the theoretical model, the influence of FRP length on the bearing capacity of RC beams strengthened with FRP was analyzed.

5) Through theoretical analysis, finite element simulation and model experiments, it can be seen that the failure modes and the strengthening effect of RC beams strengthened with FRP are determined by interfacial mechanical behaviors.

Acknowledgments

References

Ahmed, O., Van Gemert, D. and Vandewalle, L. (2001), "Improved model for plate-end shear of CFRP strengthened RC beams", *Cement Concrete Compos.*, **23**, 3-19.

Al-Zaid Rajeh, Z., Al-Negheimish Abdulaziz, I., Al-Saawani Mohammed, A. and El-Sayed Ahmed, K. (2012), "Analytical study on RC beams strengthened for flexure with externally bonded FRP reinforcement", *Compos. Part B: Eng.*, **43**(2), 129-141

Attari, N., Amziane, S. and Chemrouk, M. (2012), "Flexural strengthening of concrete beams using CFRP, GFRP and hybrid FRP sheets", *Constr. Build. Mater.*, **37**, 746-757.

Bennati, S., Dardano, N. and Valvo, P.S. (2012), "A mechanical model for FRP-strengthened beams in bending", *Frattura ed Integrità Strutturale*, **22**, 39-55.

Bilotta, A., Faella, C., Martinelli, E. and Nigro, E. (2013), "Design by testing procedure for intermediate debonding in EBR FRP strengthened RC beams", *Eng. Struct.*, **46**, 147-154.

Bizindavyi, L. and Neale, K.W. (1999), "Transfer lengths and bond strengths for composites bonded to concrete", *J. Compos. Mater. Constr.*, **3**(4), 153-160.

Bocciarelli, M. and Pisani, M.A. (2015), "Modified force method for the nonlinear analysis of FRP reinforced concrete beams", *Compos. Struct.*, **131**, 645-653.

Brena, S.F., Bramblett, R.M., Wood, S.L. and Kreger, M.E. (2003), "Increasing flexural capacity of reinforced concrete beams using carbon fiber-reinforced polymer composites", *ACI Struct. J.*, **100**(1), 36-46.

Burgueño, R., Karbhari, V.M., Seible, F. and Kolozs, R.T. (2001), "Experimental dynamic characterization of an FRP composite bridge superstructure assembly", *J. Compos. Struct.*, **54**, 427-444.

Chen, J.F. and Teng, J.G. (2001), "Anchorage strength models for FRP and steel plates bonded to concrete", *J. Struct. Eng.*, **127**(7), 784-791.

Cheng, C. and Zhu, Y. (2005), *Elastic Mechanics*, Shanghai: Shanghai University Press. (in Chinese)

Code for design of concrete structures (2010), GB-50010, China Building Industry Press, Beijing.

Diab, H. and Wu, Z. (2007), "Nonlinear constitutive model for time-dependent behavior of FRP-concrete interface", *Compos. Sci. Tech.*, **67**(11-12), 2323-2333.

Ferrier, E. and Hamelin, P. (2002), "Long-time concrete-composite interface characterization for reliability prediction of RC beam strengthened with FRP", *Mater. Struct., Materiaux et Constructions*, **35**(253), 564-572.

Gao, B., Kim, J.K. and Leung, C.K.Y. (2006), "Strengthening efficiency of taper ended FRP strips bonded to RC beams", *Compos. Sci. Tech.*, **66**(13), 2257-2264.

Guenaneche, B., Krour, B., Tounsi, A., Fekrar, A. and Benyoucef, S. (2010), "Elastic analysis of interfacial stresses for the design of a strengthened FRP plate bonded to an RC beam", *Int. J. Adhes. Adhesiv.*, **30**(7), 636-642.

Hag-Elsafi, O., Alampalli, S., Kunin, J. and Conway, T. (2004), "Timothy conway. strengthening of a concrete T-beam bridge using FRP composite laminates", *Adv. Tech. Struct. Eng.*, doi: 10.1061/40492(2000)70.

Irshidat, M.R., Al-Saleh, M.H. and Almashagbeh, H. (2016), "Effect of carbon nanotubes on strengthening of RC beams retrofitted with carbon fiber/epoxy composites", *Mater. Des.*, **89**, 225-234.

Ko, H., Matthys, S., Palmieri, A. and Sato, Y. (2014), "Development of a simplified bond stress–slip model for bonded FRP-concrete interfaces", *Constr. Build. Mater.*, **68**, 142-157.

Lin, X. and Zhang, Y.X. (2013), "Bond-slip behaviour of FRP-reinforced concrete beams", *Constr. Build. Mater.*, **44**, 110-117.

Lu, X.Z. (2004), *Studies on FRP-Concrete Interface*, Tsinghua University, Beijing. (in Chinese)

Lu, X.Z., Teng, J.G., Ye, L.P. and Jiang, J.J. (2005), "Bond-slip models for FRP sheets/plates bonded to concrete", *Eng. Struct.*, **27**(6), 920-37.

Mitolidis, G.J., Salonikios, T.N. and Kappos, A.J. (2012), "Tests on RC beams strengthened at the span with externally bonded polymers reinforced with carbon or steel fibers", *J. Compos. Constr.*, **16**(5), 551-562.

Nardini, V., Guadagnini, M. and Valluzzi, M.R. (2008), "Anchorage strength models for end-debonding predictions in RC beams strengthened with FRP composites", *Mech. Compos. Mater.*, **44**(3), 257-268

Neubauer, U. and Rostasy, F.S. (1999), "Bond failure of concrete fiber reinforced polymer plates at inclined cracks-experiments and fracture mechanics model", *Proc. of 4th International Symposium on Fiber Reinforced Polymer Reinforcement for Reinforced Concrete Structures*, Michigan, ACI, 369-382.

Protchenko, K., Wlodarczyk, M. and Szmigiera, E. (2015), "Investigation of behavior of reinforced concrete elements strengthened with FRP", *Procedia Eng.*, **111**, 679-686.

Rasheed, H.A. and Motto, N.H. (2010), "Strength design equations for FRP-strengthened concrete beams", *Australian J. Struct. Eng.*, **11**(2), 103-116.

Rostasy, F.S., Hankers, C. and Ranisch, E.H. (1992), "Strengthening of R/C and P/C structures with bonded FRP plates", *Advanced Composite Materials in Bridges and Structures, CSCE*, Sherbrooke, Canada, 253-263.

Said, H. (2010), "Deflection prediction for FRP-strengthened concrete beams", *J. Compos. Constr.*, **14**(2), 244-248.

Saxena, P., Toutanji, H. and Noumowe, A. (2008), "Failure analysis of FRP-strengthened RC beams", *J. Compos. Constr.*, **12**(1), 2-14.

Taleb, S.A. and Salem, A.S. (2015), "Bending and shear behavior of a composite beam strengthened and double-confined with FRP-jacket", *Procedia Eng.*, **114**, 165-172.

Teng, J.G. and Yao, J. (2007), "Plate end debonding in FRP-plated RC beams-II: Strength model", *Eng. Struct.*, **29**(10), 2472-2486

Zhang, S.S. and Teng, J.G. (2014), "Finite element analysis of end cover separation in RC beams strengthened in flexure with FRP", *Eng. Struct.*, **75**, 550-560.

Zhou, Y.W., Wu, Y.F. and Yun, Y. (2010), "Analytical modeling of the bond-slip relationship at FRP-concrete interfaces for adhesively-bonded joints", *Compos. Part B: Eng.*, **41**(6), 423-433.

CC